Distinct Regulation of Bioenergetics and Translation by Group I mGluRs and NMDARs

Sudhriti Ghosh Dastidar[1,2], Sumita Chakraborty[1], Sumantra Chattarji[1,3], Aditi Bhattacharya[1], Ravi S Muddashetty[1,4,*]

[1]Institute for Stem Cell Sciences and Regenerative Medicine, Bangalore, India

[2]Manipal Academy of Higher Education, Manipal, India

[3]National Center for Biological Sciences, Bangalore, India

[4] Lead Contact

* Correspondence: ravism@instem.res.in

Abstract

Neuronal activity is responsible for disproportionally large consumption of energy by the brain. However, little is known about the processes within neurons responsible for such abundant ATP outlay. Here we provide evidence that major fraction of ATP consumed on glutamate stimulation is due to activation of global *de-novo* protein synthesis mediated by group I mGluRs in cultured cortical neurons. We found mGluR and NMDAR stimulation impacts translation with distinct kinetics; while mGluR lead to rapid and sustained translation activation as measured by eEF2 phosphorylation and metabolic labeling, NMDAR stimulation induced a robust translation inhibition. Our observations established an inverse correlation between the kinetics of translation and change in ATP level for both receptors. We observed an immediate mGluR mediated reduction in neuronal ATP level while NMDA lead to a delayed (≥15 mins) protein synthesis dependent ATP expenditure demonstrating a possibility for NMDAR dependent delayed translation activation. Interestingly, we identified that AMP activated protein kinase (AMPK) has a central role in regulating downstream effects of both mGluR and NMDAR. AMPK activity was reduced on mGluR stimulation even under low ATP levels while there was a rapid increase in AMPK activity on NMDAR stimulation. Perturbing AMPK function prior to either stimulation led to a complete loss of stimulation specific effects on eEF2 phosphorylation and global translation. Our observation therefore established a pivotal role for AMPK-eEF2 signaling axis on receptor specific regulation of global translation.

Introduction

Brain is known to consume significant fraction of the body's metabolic energy even at the 'resting' state (Mink, Blumenschine, and Adams 1981). The consumption is known to increase further on neuronal activity. Evidences from FMRI based studies and PET studies with various tracer molecules have established direct correlations between brain activity and enhanced resource consumption. Conditions such as hypoglycemia and cerebral ischemia leads to severe consequences largely due to perturbations in energy supply (Rooijackers et al. 2016)(Schurr 2002). Dysregulated energy metabolism is at the heart of conditions such as epilepsy and various neuro-degenerative diseases (Koenig and Dulla 2018)(Vallée et al. 2018). Therefore, highly regulated energy management is a key requirement for proper cognitive functions of the brain.

Synapses are thought to be the sites of major ATP consumption (Attwell and Laughlin 2001)(Harris, Jolivet, and Attwell 2012) due to large number of cellular processes being activated on arrival of a stimulus. While high rate of endocytosis is reported to consume maximum energy at the pre-synaptic boutons on electrical stimulation (Rangaraju, Calloway, and Ryan 2014)(Pathak et al. 2015), our understanding is quite limited as to what extent various processes consume ATP at the post-synaptic compartments and at the pan-neuronal context. Neuronal activity has also been known to induce abundant protein synthesis (Rangaraju, tom Dieck, and Schuman 2017), a determining resource for long term synaptic plasticity and memory formation. Since each round of amino acid incorporation requires 4 ATP molecules along with additional ATP required for amino

acid charging and initiation (Schwanhüusser et al. 2011)(Rangaraju, tom Dieck, and Schuman 2017), any change therefore in the rate of global protein synthesis is expected to have a reflection on the steady state ATP level. Group I metabotropic glutamate receptors (mGluRs referred hereafter) and NMDARs are widely implicated to facilitate or induce various forms of synaptic plasticity across different brain regions (Hunt and Castillo 2012)(Malenka 2012). While mGluRs are known to activate translation rapidly (Huber, Kayser, and Bear 2000)(Luchelli, Thomas, and Boccaccio 2015), NMDAR stimulation causes translation inhibition at an immediate time scale (Scheetz, Nairn, and Constantine-paton 2000). Considering the distinct nature of their downstream regulation, it would therefore be interesting to understand the impact of mGluR and NMDAR activation on cellular energetics.

Neuronal activity is also known to trigger ATP production through activation of glycolysis and oxidative phosphorylation (Rangaraju, Calloway, and Ryan 2014)(Marinangeli et al. 2018)(Manlio Díaz-García et al. 2017)(Rangaraju, Lauterbach, and Schuman 2019) to support the enhanced consumption. One key molecular player in such a scenario would be AMP activated protein kinase (AMPK). AMPK is a known sensor for cellular ATP/AMP ratio and acts to balance various catabolic and anabolic processes including global translation (Burkewitz, Zhang, and Mair 2014). AMPK activation has been shown to be critical to support synaptic ATP level on neuronal activity (Marinangeli et al. 2018) and influence various forms synaptic plasticity (Potter et al. 2010)(Kong et al. 2016). Thus, understanding how AMPK coordinates activity dependent changes on energetics and translation is of paramount importance. To gain deeper insight, we therefore addressed the following questions: 1) How is the energy level altered over

time on synaptic activity 2) What are the mechanisms crucial for dynamic regulation of translation on activation of mGluRs and NMDARs and 3) How AMPK activity is altered to strike a balance between energy and translation regulation under such scenario.

Here we report that stimulation with glutamate, the major neurotransmitter in vertebrate CNS, causes large amount of energy consumption primarily due to the activation of global translation by mGluRs at post synapse and globally throughout the neuron. We also report a distinct difference in the kinetics of translation regulation induced by mGluRs and NMDARs. These distinct responses in turn depend on the differential activation of AMPK downstream of mGluRs and NMDARs involving mechanisms mutually exclusive. Finally, we show that acute perturbations of AMPK function lead to complete loss of translation regulation on both stimulations thereby establishing AMPK as biochemical coupling mechanism between energetics and translation on neuronal activity.

Results:

mGluR Dependent Protein Synthesis Consumes Significant Fraction of Neuronal ATP Following Glutamate Stimulation:

To assess the impact of translation on global ATP levels, we used cultured cortical neurons from Sprague Dawley (SD) rats and stimulated with glutamate (25μM) for 5 minutes at day *in vitro* 15 (DIV 15) in presence or absence of protein synthesis inhibitors anisomycin or cycloheximide. We then quantified the ATP/(ATP+ADP) ratio from cell lysates using bioluminescence-based methods (**Figure 1A**). Glutamate Stimulation alone led to significant reduction in the neuronal ATP/(ATP+ADP) ratio. This stimulation

dependent reduction was absent in presence of protein synthesis inhibitors anisomycin (25μM) or cycloheximide (100μg/ml) (**Figure 1B**) while drugs themselves had no significnat impact on the ATP/(ATP+ADP) ratio. These observations suggest a large increase in protein synthesis on stimulation, responsible for consuming signifcant fraction of neuronal ATP. The identical effects of both anisomycin and cycloheximide negates the possibility of these observations due to non-specific effects of these drugs.

Further, to understand the contributions from individual glutamate receptors, we repeated glutamate stimulation inhibiting either ionotropic NMDA and AMPA receptors with a cocktail of D-AP5 (25μM) + CNQX (40μM) (referred to as inotropic glutamate receptor (iGluR) blocker cocktail hereafter) or inhibiting mGluRs with MPEP (10μM). Co-stimulation with iGluR blocker cocktail led to significant reduction in ATP/(ATP+ADP) ratio similar to glutamate alone while stimulation along with MPEP abolished the glutamate mediated reduction significantly (**Figure 1C**). These results therefore, indicate that the observed reduction in ATP on glutamate stimulation is majorly due to mGluR activity with minimal contributions from the iGluRs. Furthermore, Stimulation in presence iGluR blocker cocktail along with protein synthesis inhibitor anisomycin removed the energy burden (**Figure 1B**) corroborating the idea of a robust increase in protein synthesis consumes significant fraction of neuronal ATP independent of iGluR activity. To further investigate on this idea, we stimulated cortical neurons with mGluR and NMDAR specific agonists s-3,5 DHPG and NMDA respectively. While DHPG treatment led to a significant reduction in ATP/ATP+ADP ratio, NMDA had no significant impact **(Supplementary figure 1A)** ascertaining the importance of mGluR activity on energy consumption. To account for the contribution from endocytosis on glutamate mediated

ATP consumption, we blocked GTP dependent enzyme dynamin with small molecule inhibitor dynasore (100μM). Stimulation in presence dynasore had identical effects as that of glutamate alone (**Supplementary figure 1B)** suggesting activity induced vesicle endocytosis has negligible effect on pan-neuronal ATP level.

To understand the impact of mGluR and NMDAR stimulation on synaptic energy level, we prepared synaptoneurosomes from whole rat cortices at post-natal day 30 (P30) and stimulated with DHPG (100μM) and NMDA (50μM) respectively (**Figure 1D**). Synaptoneurosome preparation was validated with enrichment of synaptic marker PSD 95 without any significant enrichment of glial marker GFAP (**Figure 1E**). Synaptic ATP levels showed significant reduction on mGluR stimulation (**Figure 1F**). The reduction in synaptic ATP levels on stimulation was abolished in presence of mGluR inhibitor MPEP, protein synthesis inhibitor anisomycin and cycloheximide (**Figure 1F**) indicating changes in synaptic ATP level on mGluR stimulation is majorly due to protein synthesis. NMDAR stimulation on the contrary had no significant effect on synaptic ATP level and was unaltered in presence of NMDAR inhibitor D-AP5 (**Figure 1F, supplementary figure 1C**). Therefore, our observations suggest mGluR dependent protein synthesis creates significant energy demand both at the synaptic and at the pan-neuronal level.

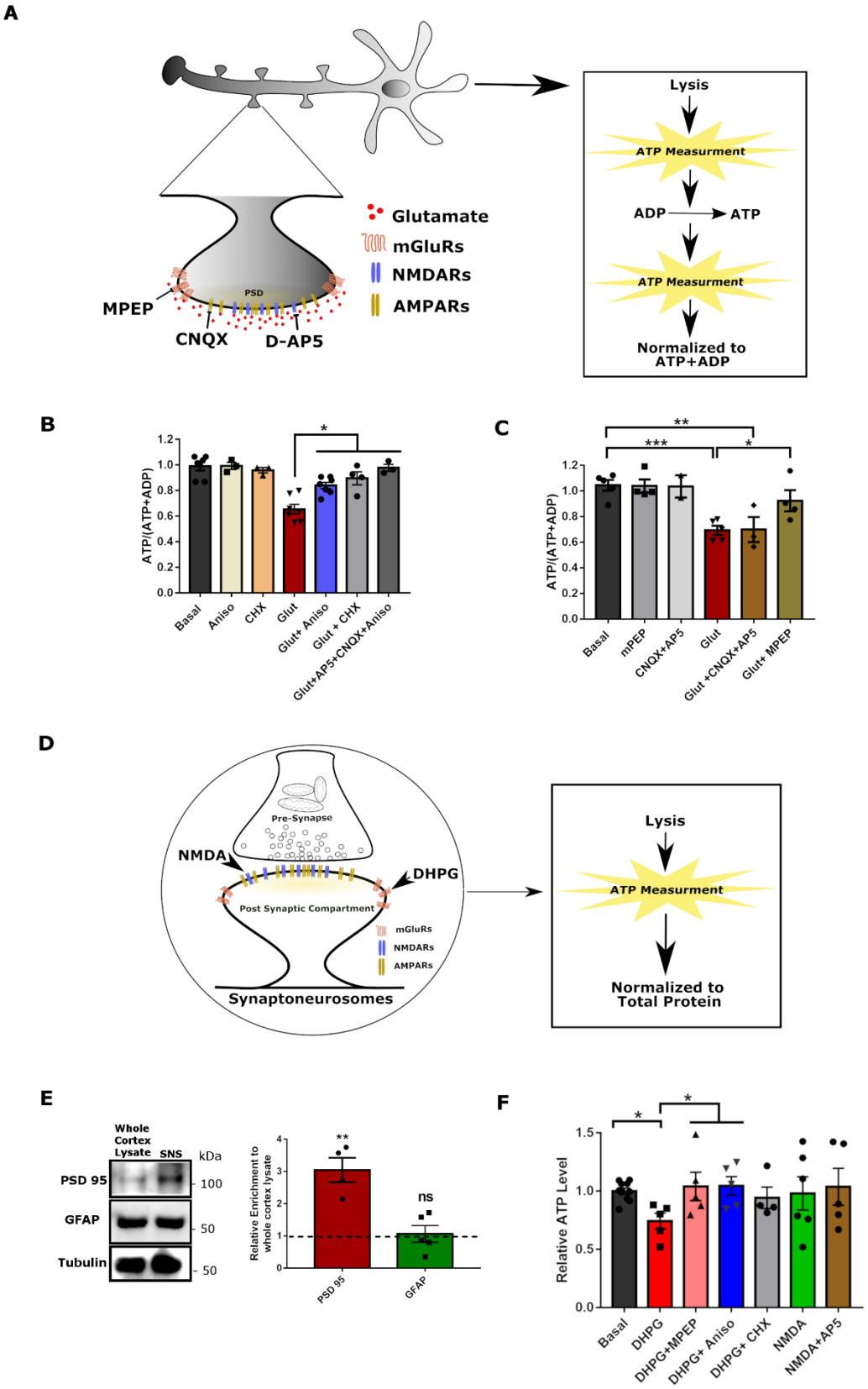

Legend for Figure 1

Glutamate Dependent Changes in Neuronal ATP/ADP Ratio is Primarily Due to Group I mGluR Dependent Protein Synthesis.

(A) Schematic depicting experimental work flow for measurement of ATP/ATP+ADP ratio from cultured cortical neurons at 15 day *in-vitro* (DIV 15) using luciferase-based methods.

(**B)** Bar graph representing normalized average value of neuronal ATP/ATP+ADP ratio in unstimulated condition, in presence of Anisomycin (25μM), cycloheximide (350μM), on glutamate (25μM) stimulation alone for 5 minutes, on glutamate stimulation along with anisomycin, on glutamate stimulation along with cycloheximide and on glutamate stimulation in combination with D-AP5, CNQX and anisomycin. Data represented as: mean ± SEM with scattered data points. *$p<0.05$, n=3-6 independent plating. One-way ANOVA followed by Bonferroni's multiple comparison test.

(**C)** Bar graph representing normalized average value of neuronal ATP/ATP+ADP ratio in unstimulated condition, in presence of MPEP (10μM), in presence of the cocktail of CNQX (40μM) + D-AP5 (25μM), on glutamate (25μM) stimulation alone for 5 minutes, on glutamate stimulation along with the cocktail of CNQX + D-AP5 and on glutamate stimulation along with MPEP. Data represented as: mean ± SEM with scattered data points. *$p<0.05$, **$p<0.01$, ***$p<0.001$, n=3-5 independent plating. One-way ANOVA followed by Bonferroni's multiple comparison test.

(D) Schematic depicting experimental work flow for measurement of synaptic ATP level from cortical synaptoneurosomes obtained from Sprague dawley rats at post-natal day 30 (P30) using luciferase-based methods.

(E) Immunoblots showing PSD 95 and GFAP levels on whole cortical lysate and synaptoneurosome preparation. Quantification representing average fold enrichment of PSD 95 and GFAP on synaptoneurosome preparations compared to whole cortex lysate.

(F) Bar graph representing normalized average value of synaptic ATP level in unstimulated condition, on DHPG (100μM) treatment for 5 minutes, on DHPG treatment along with MPEP (10μM), on DHPG treatment along with anisomycin (50μM), on DHPG treatment along with cycloheximide (350μM), on NMDA (40μM) treatment for 5 minutes and on NMDA treatment along with D-AP5 (25μM). Data: mean +/- SEM with scattered data points. *$p<0.05$, n=5-10 independent plating. One-way ANOVA followed by Bonferroni's multiple comparison test.

mGluRs and NMDARs Impact Synapto-dendritic ATP Levels with Distinct Kinetics

To understand the kinetics of activity induced changes in energy level at a more compartment specific manner, we measured ATP/ADP ratio following mGluR and NMDAR stimulation at the distal dendrites of cortical neurons (~50μm away from cell body) using ratio sensor PercevalHR as reported previously (Tantama et al. 2013) (**Figure 2A**). Perceval pH bias was approximately corrected by simultaneous measurement of intracellular pH with the ratio sensor pH-Red using the linear relation established between Perceval and pH-Red fluorescence as described previously (Pedersen et al. 1998)(Tantama et al. 2013) **(supplementary figure 2A)**. On bath application of 50μM DHPG, we observed a rapid and significant reduction (~ by 2 mins) in the dendritic ATP/ADP ratio. The ratio continued to stay low long as DHPG was present in the media (**Figure 2B-2E**). Application of NMDA (20μM) on bath conversely showed much delayed (~10 minutes post-stimulation) reduction in the ratio indicating a slow kinetics of NMDAR effect on dendritic ATP:ADP ratio distinctly different to that

of mGluRs (**Figure 2B-2E)**. Stimulation in presence of protein synthesis inhibitor anisomycin inhibited the activity dependent reduction in the dendritic ATP/ADP ratio for both DHPG and NMDA treatment (**Figure 2C-2F**). While the dendritic ATP/ADP ratio was unaltered under basal condition, application of anisomycin led to a sharp rise in ATP/ADP ratio reflecting the energy consumption due to basal protein synthesis (**supplementary figure 2B and 2C**). Our observations therefore clearly indicate that stimulation dependent protein synthesis is a major energy burden even at the local dendritic compartments.

To investigate the kinetics of ATP regulation at the synapse we used cortical synaptoneurosome preparation. We stimulated synaptoneurosomes for 1, 2 and, 5 minutes and allowed recovery for 5 minutes after stimulation (hence referred to as 5 min recovery hereafter). ATP levels were quantified from the specified time points using luminescence-based methods from synaptoneurosomal lysates (**Figure 2F**). DHPG (100μM) addition alone led to a rapid and significant reduction of the synaptic ATP level at 2 minutes and 5 minutes after stimulation and reached baseline at 5 min recovery time point. The DHPG induced changes in synaptic ATP levels was lost in presence of anisomycin highlighting most of the change in the ATP level was contributed by protein synthesis (**Figure 2G**). NMDA stimulation in the same system had no significant impact on the ATP levels till 5 minutes of stimulation but exhibited a significant reduction at 5 min recovery time point. Stimulation in presence of anisomycin had no additional effect as that of NMDAR alone (**Figure 2H**) suggesting no detectable amount of protein synthesis happened till 5 minutes of NMDAR stimulation (Scheetz, Nairn, and Constantine-paton 2000). Synaptic ATP level was unaltered in absence of any

stimulation for a period similar as stimulations (**supplementary figure 2D**). Together our results indicate mGluR stimulation leads to a rapid and persistent reduction in ATP level in a protein synthesis dependent manner while NMDAR stimulation impacts ATP level with a late onset of protein synthesis.

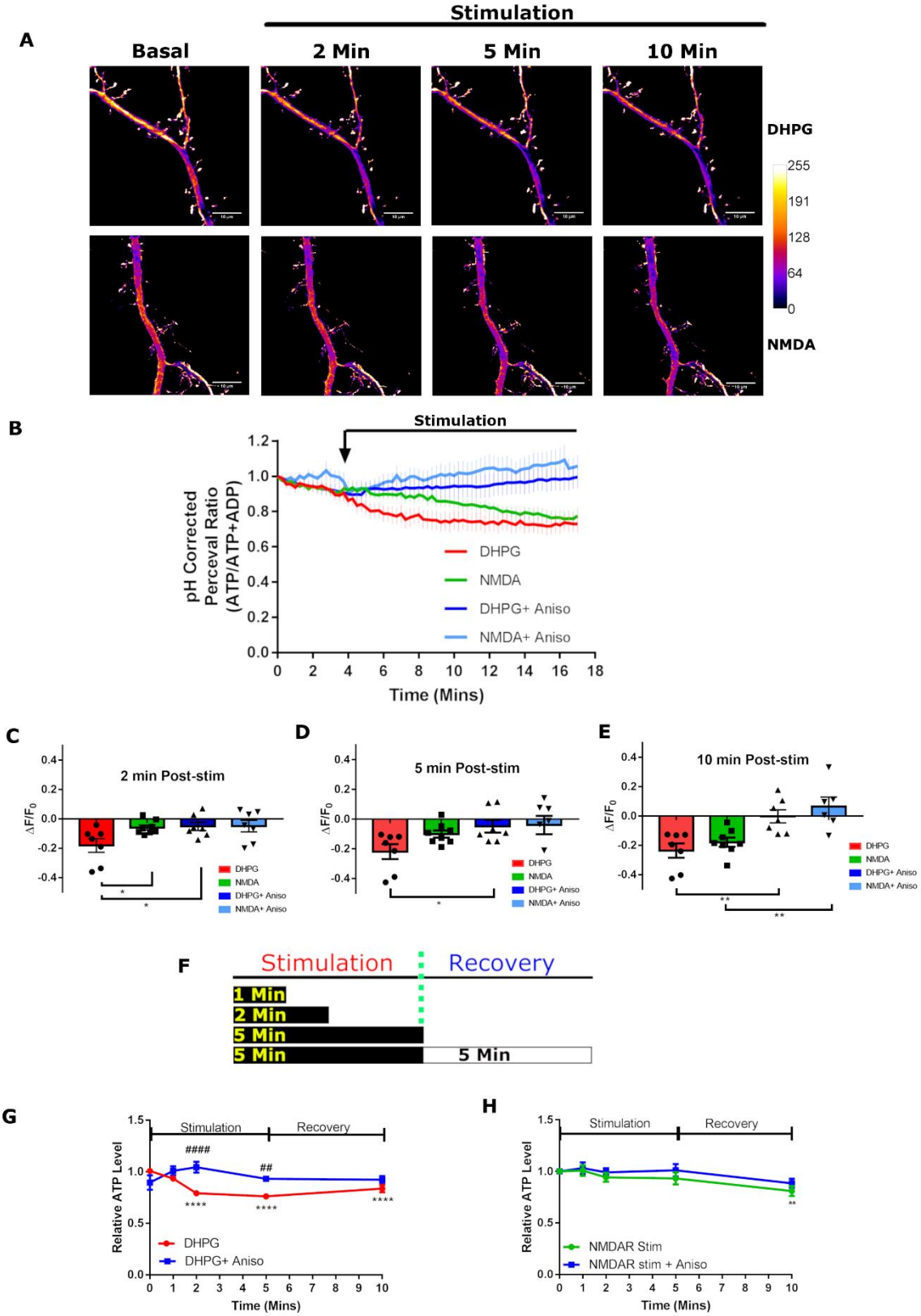

Legend for Figure 2

mGluRs and NMDARs Impact Synapto-dendritic ATP/ADP Ratio with Distinct Kinetics.

(A) Representative dendrite showing changes on PercevalHR fluorescence ratio (~ATP/ADP ratio) on bath application of DHPG (50μM) and NMDA (20μM). Scale=10μM.

(B) Average time traces showing the changes in the dendritic ATP/ADP ratio on DHPG and NMDA treatment in presence or absence of anisomycin (25μM). The curved arrow on top indicates the time when stimulants were added and kept in the imaging media. Data: mean +/- SEM, n= 6-8 cells from independent plating.

(C) Bar graph representing average change in PercevalHR fluorescence (ΔF/F) on DHPG treatment, NMDA treatment, DHPG treatment along with anisomycin and NMDA treatment along with anisomycin 2 minutes after stimulant was added on bath. Data: mean +/- SEM. *p<0.05, n= 6-8 cells from independent plating. One Way ANOVA followed by Bonferroni's multiple comparison test.

(D) Bar graph representing average change in PercevalHR fluorescence (ΔF/F) on DHPG treatment, NMDA treatment, DHPG treatment along with anisomycin and NMDA treatment along with anisomycin 5 minutes after stimulant was added on bath. Data: mean +/- SEM. *p<0.05, n= 6-8 cells from independent plating. One Way ANOVA followed by Bonferroni's multiple comparison test.

(E) Bar graph representing average change in PercevalHR fluorescence (ΔF/F) on DHPG treatment, NMDA treatment, DHPG treatment along with anisomycin and NMDA treatment along with anisomycin 2 minutes after stimulant was added on bath. Data: mean +/- SEM. **p<0.01, n= 6-8 cells from independent plating. One Way ANOVA followed by Bonferroni's multiple comparison test.

(F) Schematic depicting stimulation protocol in cortical synaptoneurosomes for quantification synaptic ATP levels.

(G) Line graph showing average synaptic ATP levels at various time points after DHPG (100μM) treatment and 5 minutes after recovery in presence or absence of anisomycin (50μM). Data: mean +/- SEM, *p<0.05, **p<0.01, ****p<0.0001 for comparison with 0 minute. ##p<0.01 and ####p<0.0001 for comparison between DHPG+aniso. n≥ 5 animals per group. Two Way ANOVA followed by Bonferroni's multiple comparison test.

(H) Line graph showing average synaptic ATP levels at various time points after NMDA (40μM) treatment and 5 minutes after recovery in presence or absence of anisomycin (50μM). Data: mean +/- SEM, **p<0.01 for comparison with 0 minute. n≥ 4 animals per group. Two Way ANOVA followed by Bonferroni's multiple comparison test

mGluRs and NMDARs Regulate eEF2 Phosphorylation to Create Distinct Kinetics of Translation

To understand the stimulation dependent changes on global translation with a direct correlate, we quantified de-novo protein synthesis at various time points after stimulation using FUNCAT metabolic labeling technique as described previously (Dieterich et al. 2010). Cortical neurons (DIV 15) were methionine starved for 1 hour followed by application of methionine analogue AHA and incubation for 1 hour for abundant labeling of proteins. This was followed by stimulation as described in figure 2F and fixation (**Figure 3A**). Newly synthesized proteins were visualized by tagging the AHA containing proteins with Alexa 555 alkyn. Mean FUNCAT intensity was then quantified from somata and dendrites representing quantity of proteins synthesized cumulatively over the period of stimulation (**Figure 3B, 3C, 3D and supplementary**

figure 3B). On bath application of DHPG, we did not observe any discernable change in the FUNCAT signal by 2 minutes. The signal increased significantly though by 5 minutes of stimulation and by 5 min recovery as compared to unstimulated cells. This demonstrates a robust and persistent increase in de-novo protein synthesis on mGluR stimulation in cultured cortical neurons (**Figure 3C and 3D**). On the contrary NMDA stimulation led to a significant reduction in FUNCAT signal compared to unstimulated cells by 2 minutes while the signal intensity returned to baseline by 5 minutes of stimulation and continued to stay unchanged till 5 min recovery (**Figure 3C and 3D**) indicating a rapid inhibition of translation on NMDAR stimulation. No significant change in FUNCAT signal was observed in absence of any stimulation (**supplementary figure 3A**). No detectable signal was observed in absence of any AHA incubation which acted as a negative control for our experiment (**supplementary figure 3A**). Therefore, our observations reveal a robust and persistent activation of translation mediated by mGluRs while NMDAR stimulation led to a rapid inhibition of translation.

Eukaryotic elongation factor 2 (eEF2) has been proposed to be a signal integrator (Sutton et al. 2007) and its phosphorylation is known to respond to various synaptic stimuli (Scheetz, Nairn, and Constantine-paton 2000)(Takei et al. 2009) thereby regulating translation elongation (Richter and Coller 2015). Phosphorylation of Thr 56 residue of eEF2 is known to reduce the rate of translation elongation thereby causing global translation inhibition (Ryazanov and Davydova 1989). To gain insight on the modes of translation regulation downstream of both receptors, we decided to investigate on the role of elongation factor 2 (eEF2) phosphorylation in cultured cortical neurons. We quantified eEF2 phosphorylation 5 minutes after stimulation, a time point

corresponding to maximum difference observed in FUNCAT signal (**Figure 3E and Supplementary figure 3C**). We observed a significant reduction in p-eEF2 levels 5 minutes after DHPG treatment as compared to unstimulated cells. NMDA treatment on the contrary robustly increased the p-eEF2 levels in the cell somata and dendrites (**Figure 3F**). Further we used phospho/ total ratio of eEF2 as a readout to gain a snapshot view of global translation in cortical synaptoneurosomes (**Figure 3G**) and in cortical neurons (**supplementary figure 3D**). Synaptoneurosomes were stimulated for different time period as mentioned before (**Figure 2F**). We observed a significant difference in the kinetics of eEF2 phosphorylation regulated by mGluR and NMDAR stimulation (**Figure 3H and supplementary figure 3E**). mGluR stimulation led to an immediate reduction in phospho/total eEF2 ratio by 1 minute. The decrease in the ratio persisted till 5 minutes of stimulation and returned to baseline by 5 mins of recovery. NMDAR stimulation, on the contrary lead to an immediate increase in the phospho/Total eEF2 ratio by 1 minute correlated well with the decrease in FUNCAT signal observed 2 minutes after stimulation in cortical neurons. The increase in the ratio persisted till 5 minutes of NMDAR stimulation and returned to baseline by 5 min recovery time point (**Figure 3H**). The ratio stayed unaltered in absence of any stimulation (**supplementary figure 4B**). Therefore, we found a strong correlation between the global translation and eEF2 phosphorylation downstream of both the glutamate receptors.

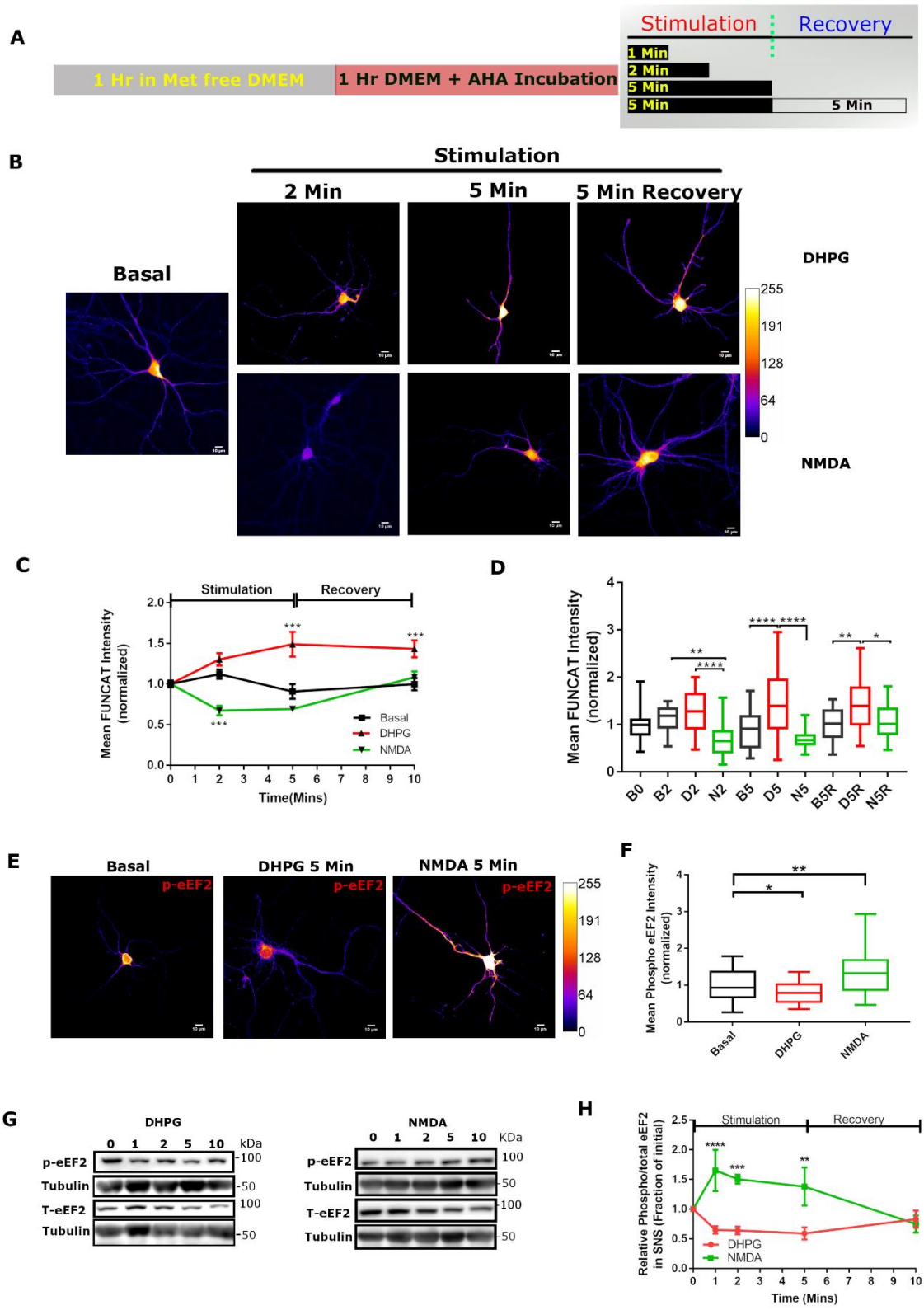

Legend for Figure 3:

mGluR and NMDAR Alter Global Translation by Regulating eEF2 Phosphorylation with Distinct Kinetics.

(A) Schematic depicting the experimental workflow and stimulation protocol to visualize and quantify newly synthesized protein on stimulation through metabolic labeling technique in cortical neurons DIV 15.

(B) Representative images showing newly synthesized proteins visualized through FUNCAT metabolic labeling (pseudo-colored) in cortical neurons at various time points following DHPG (50μM) and NMDA (20μM) treatment. MAP2B immunolabeling (supplementary figure 3B) was used for identifying neurons and intensity was used for normalization. Scale=10μM.

(C) Line graph showing average amount of newly synthesized protein before stimulation (basal) and at various time points following DHPG and NMDA treatments. Data: mean +/- SEM, ***p<0.001 n= 21-54 neurons per group from 3 independent plating. Two Way ANOVA followed by Bonferroni's multiple comparison test.

(D) Box plot showing distribution of data points for the newly synthesized protein obtained from various neurons for each group. *p<0.05, **p<0.01, ***p<0.001, ****p<0.0001, n= 21-54 neurons per group from 3 independent plating. One Way ANOVA followed by Bonferroni's multiple comparison test.

(E) Representative images showing phospho-eEF2 immunolabeling (Pseudo-colored) in cortical neurons on basal, DHPG and NMDA treatments for 5 minutes. MAP2B immunolabeling (supplementary figure 3C) was used for identifying neurons and intensity was used for normalization. Scale=10μM.

335 **(F)** Box plot showing phospho-eEF2 intensity distribution across multiple neurons on basal
336 condition and on DHPG and NMDA treatment for 5 minutes. *p<0.05, **p<0.01, n=31-49 cells per
337 group from 3 independent plating. One-way ANOVA followed by Bonferroni's multiple
338 comparison test.

339 **(G)** Representative immunoblots describing changes in phospho-eEF2 and total-eEF2 levels at
340 various time points after DHPG (100μM) and NMDA (40μM) treatment to cortical
341 synaptoneurosomes. Note in each case phospho and total eEF2 levels were normalized
342 individually to tubulin before calculating the ratio.

343 **(H)** Line graph showing average value for synaptic phospho/total ratio of eEF2 at various time
344 points after DHPG and NMDA treatment and 5 minutes after recovery. Data: mean +/- SEM,
345 **p<0.01, ***p<0.001, ****p<0.0001, n≥ 5 animals per group. Two Way ANOVA followed by
346 Bonferroni's multiple comparison test.

347 **mGluRs and NMDARs Regulate AMPK Activity in Contrasting Manner**

348 AMP activated protein kinase (AMPK) is a widely studied global sensor for ATP/AMP or
349 ATP/ADP ratio and is known to regulate various catabolic and anabolic processes during
350 energy stress (Burkewitz, Zhang, and Mair 2014). Since mGluRs and NMDARs had
351 contrasting effect on both ATP/ADP ratio and global translation, we sought to
352 understand if AMPK activity was altered to achieve stimulation specific effects. To
353 examine the global status of AMPK activity we quantitated T172 phosphorylation on
354 AMPK α subunit 5 minutes after stimulation in cortical neurons through immunolabeling
355 (DIV 15) (**Figure 4A and supplementary figure 4A**). T172 is present in the activation
356 loop of AMPK and its phosphorylation is positively correlated with heightened AMPK
357 activation (Hawley et al. 1996). We observed a significant decrease in p-AMPK

immunolabeling on mGluR stimulation compared unstimulated condition. NMDAR stimulation on the contrary led to a significant rise in the immunolabel indicating an increase in AMPK activity (**Figure 4B**). To understand the temporal changes in AMPK activity, we stimulated cortical synaptoneurosomes with DHPG followed by measurement of phospho/total AMPK ratio (**Figure 4C**). We found a significant decrease in the ratio by about 2 minutes after DHPG treatment persisting till 5 minutes of recovery (**Figure 4D**) while the ratio stayed unaltered in absence of any stimulation (**supplementary figure 4B**). These results indicate that AMPK activity underwent reduction on mGluR stimulation despite an observed decline in the ATP level. Surprisingly, the mGluR mediated reduction in AMPK activity was found to be abolished in presence of anisomycin underscoring the importance of de-novo protein synthesis in regulation of AMPK activity (**Figure 4C and 4D)**. One pressing idea was therefore to test whether mGluR stimulation leads to synthesis of any protein that would inhibit AMPK phosphorylation. We chose α-SNAP, a *cis*-SNARE disassembly factor, as a potential candidate to investigate on its role in inhibiting AMPK as it is previously reported to act as an AMPK phosphatase (Wang and Brautigan 2013). We investigated the α-SNAP protein level on DHPG treatment in cortical synaptoneurosomes (**Figure 4E**). A significant increase in α-SNAP level was observed on 1 min of DHPG addition and was persistent till 5 min recovery (**Figure 4F**), a temporal feature well correlated with AMPK inactivation kinetics (**Figure 4D**). The DHPG induced increase in α-SNAP level was found to be abolished in presence of protein synthesis inhibitor anisomycin indicating mGluR dependent de-novo synthesis of α-SNAP plays a critical role in AMPK dephosphorylation (**Figure 4F**). Further We quantified the association between α-SNAP and AMPK on mGluR

stimulation in cortical cultured neurons (**Figure 4G**) as α-SNAP is known to stabilize the de-phosphorylated version of AMPK. We observed a significant increase in colocalization between α-SNAP and AMPK in cortical neurons after DHPG treatment (5 minutes) compared to unstimulated condition (**Figure 4H**). These results therefore suggest a crucial role for protein α-SNAP in mediating mGluR mediated dephosphorylation of AMPK.

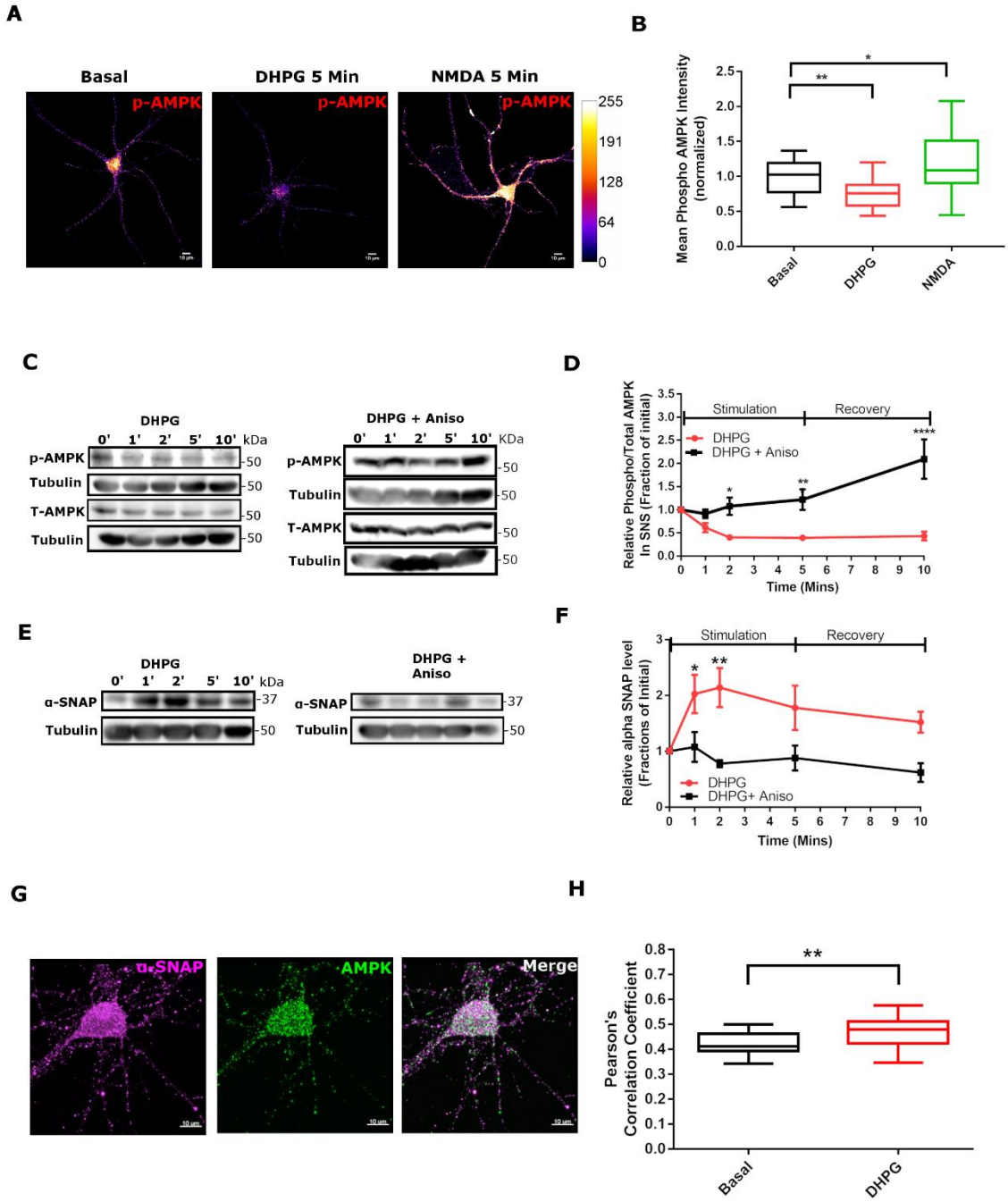

Legend for Figure 4:

mGluR Inhibit While NMDAR Activate AMPK to Regulate Translation.

(A) Representative images showing phospho-AMPK immunolabeling (Pseudo-colored) in cortical neurons on basal, DHPG and NMDA treatments for 5 minutes. MAP2B immunolabeling (supplementary figure 4A) was used for identifying neurons and intensity was used for normalization. Scale=10μM.

(B) Box plot showing phospho-AMPK intensity distribution across multiple neurons on basal condition and on DHPG and NMDA treatment for 5 minutes. *p<0.05, **p<0.01, n=30-46 cells per group from 3 independent plating. One-way ANOVA followed by Bonferroni's multiple comparison test.

(C) Representative immunoblots describing changes in phospho-AMPK and total-AMPK levels at various time points after DHPG (100μM) treatment to cortical synaptoneurosomes in presence or absence of anisomycin (50μM). Note in each case phospho and total AMPK levels were normalized individually to tubulin before calculating the ratio.

(D) Line graph showing average value for synaptic phospho/total ratio of AMPK at various time points after DHPG treatment and 5 minutes after recovery in presence or absence of anisomycin. Data: mean +/- SEM, *p<0.05, **p<0.01, ****p<0.0001, n= 5 animals per group. Two Way ANOVA followed by Bonferroni's multiple comparison test.

(E) Representative immunoblots depicting changes in α-SNAP levels at various time points after DHPG treatment to cortical synaptoneurosomes in presence or absence of anisomycin.

(F) Line graph showing average value for synaptic α-SNAP levels at various time points after DHPG treatment and 5 minutes after recovery in presence or absence of anisomycin. Data:

mean +/- SEM. *p<0.05, **p<0.01, n≥ 4 animals per group. Two Way ANOVA followed by Bonferroni's multiple comparison test.

(G) Representative images showing α-SNAP (green) and AMPK (red) immunolabeling in cortical neurons. Merge shows the colocalization of two channels. Scale=10μM.

(H) Box plot depicting quantification of co-localization between ά-SNAP and AMPK in cortical neurons under basal and DHPG treated conditions. **p<0.01, n≥24 cells per group from 3 independent plating. Unpaired-sample t test.

NMDAR Regulate AMPK Activity in Ca2+ Dependent Manner

We further investigated the kinetics and mechanism of NMDAR mediated AMPK regulation in cortical synaptoneurosomes (**Figure 5A**). We observed a rapid increase in phospho/total AMPK ratio by 1 minute of stimulation and persisting till 5 mins recovery (**Figure 5B**). This observation is in parallel to our previous observation in neurons where NMDA stimulation lead to enhanced phosphorylation of AMPK (**Figure 4B**). Interestingly we did not observe any detectable change in ATP level (**Figure 2I**) at a similar time scale hinting towards an ATP independent regulation of AMPK. CamKIIß, one of the upstream kinases of AMPK (Burkewitz, Zhang, and Mair 2014)(Burkewitz et al. 2014), is known to phosphorylate it in a Ca^{2+} dependent and ATP independent manner. Therefore, we hypothesized that NMDAR dependent increase in AMPK function is mediated by increased cytosolic Ca^{2+} levels entered through open NMDARs. To test the hypothesis, we repeated NMDAR stimulation in absence of extracellular Ca^{2+} (**Figure 5A**). We observed a significant difference in AMPK response on NMDA treatment in absence of extracellular Ca^{2+}. The stimulation dependent increase in phospho/total AMPK ratio was absent in Ca^{2+} free buffer underscoring the importance of Ca^{2+} signaling

433 in this context (**Figure 5B**). Interestingly we observed the NMDA dependent increase in
434 phspho/total eEF2 level was also abolished in absence of extracellular Ca^{2+}
435 (**supplementary figure 4D**) clearly demonstrating the importance of Ca^{2+} dependent
436 signaling mechanism in NMDAR dependent translation regulation.

437 We further followed the kinetics of NMDAR mediated Ca^{2+} entry in cortical neurons.
438 Cytosolic free Ca^{2+} level was quantified on NMDAR stimulation using fluorescent based
439 Ca^{2+} probe Fluo-8AM. We observed a rapid increase in Fluo8 fluorescence on NMDA
440 addition and persisted till the presence of stimulant in the media (**Figure 5C, 5F and**
441 **5G**) indicating an increase in intracellular Ca^{2+} on NMDA treatment. The amount of Ca2+
442 entered was non-saturating as could be inferred from further increase in fluorescence
443 on addition of ionomycin in presence of 10mM Ca^{2+} (**Figure 5F**). The observed increase
444 in Ca^{2+} is NMDA specific as pre-treatment with D-AP5 abolished the rise in Ca^{2+} (**Figure**
445 **5D, 5F and 5G**). The Ca^{2+} surge is contributed primarily by synaptic NMDARs as the
446 response was observed to be absent in presence of MK801 (10μM), a compound known
447 to block the open NMDAR channel pores (**supplementary figure 4C; Figure 5G**). The
448 rise in fluorescence on stimulation was abolished in the absence of extracellular Ca^{2+}
449 indicating the source of the ions are majorly extracellular in nature (**Figure 5E, 5F and**
450 **5G**). Therefore, our results indicate NMDAR mediated rapid entry of external Ca^{2+} is
451 responsible for rapid AMPK activation.

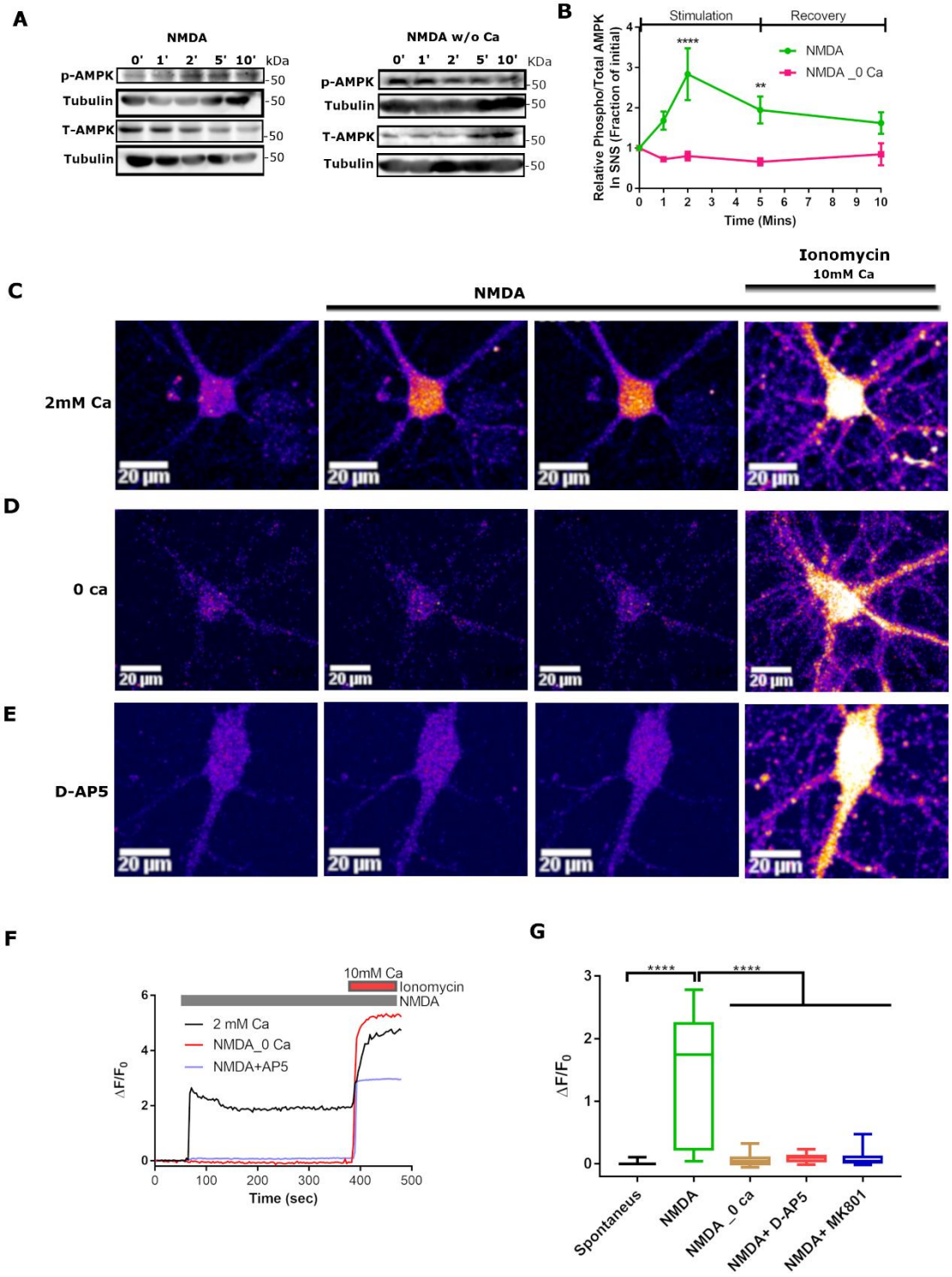

Legend for Figure 5:

NMDAR Regulate AMPK Activity in Ca2+ Dependent Manner

(A) Representative immunoblots describing changes in phospho-AMPK and total-AMPK levels at various time points after NMDA (40μM) treatment to cortical synaptoneurosomes in presence or absence of extracellular Ca^{2+}. Note in each case phospho and total AMPK levels were normalized individually to tubulin before calculating the ratio.

(B) Line graph showing average value for synaptic phospho/total ratio of AMPK at various time points after NMDA treatment and 5 minutes after recovery in presence or absence of extracellular Ca^{2+}. Data: mean +/- SEM, **p<0.01, ****p<0.0001, n= 6 animals per group. Two Way ANOVA followed by Bonferroni's multiple comparison test.

(C,D,E) Representative images depicting intracellular Ca^{2+} levels (Pseudo-colored) of a cortical neuron before stimulation, immediately (15s) after NMDA (20μM) treatment, at a later time point (300sec) after NMDA treatment and after ionomycin treatment along with 10mM Ca^{2+} in presence or absence of extracellular Ca^{2+} and D-AP5. Scale=20μM.

(F) Representative time trace showing the change in Fluo8 fluorescence on NMDA treatment in presence or absence of extracellular Ca^{2+} and D-AP5. Ionomycin treatment in presence of 10mM Ca^{2+} was used to calculate fluorescence maximum for a particular cell.

(F) Box plot showing the distribution of $\Delta F/F_0$ across multiple neurons under spontaneously firing condition, on NMDA treatment in presence or absence of Ca^{2+}, on NMDA treatment along with D-AP5 (25μM) and on NMDA treatment along with MK-801. ****p<0.0001, n≥30 neurons per group from 3 independent plating. One-way ANOVA followed by Bonferroni's multiple comparison test.

Perturbation of AMPK Function Disrupts mGluR and NMDAR Specific Translation Response

We present two key pieces of experimental evidence to verify the idea that tight regulation of AMPK function is necessary to generate receptor specific translation response. Since mGluR activation lead to inhibition of AMPK function, first we hypothesized that acute activation of AMPK with 5-aminoimidazole-4-carboxamide ribonucleotide (AICAR; 1mM) should preclude the mGluR specific effect on translation. AICAR treatment alone led to significant increase in p-eEF2 levels (**Figure 6B, supplementary 5A)** without any significant alteration in FUNCAT signal (**Figure 6D, supplementary 5A**) in cortical neurons. These observations establish a direct influence imparted by AMPK on eEF2 phosphorylation and on global translation. Supporting this hypothesis, DHPG mediated reduction in p-eEF2 level was abolished (**Figure 6A,B, supplementary figure 5B**) and DHPG induced increase in global translation was absent in presence of AICAR (**Figure 6C,D, supplementary figure 5B**). Next, we examined the impact of AMPK inhition on NMDAR stimulation using AMPK inhibitor Compund C (Dorsomorphin). Blocking AMPK function with Compound C (Dorsomorphin) had no significant impact on basal p-eEF2 level (**6F, supplementary 5A**) and but led to a significant increase FUNCAT signal (**6H, supplementary 5A**). Interestingly, NMDA application in presence of Compound C completely abolished the NMDA mediated increase in p-eEF2 level (**Figure 6E,F, supplementary figure 5C**) and also diminished the NMDA mediated inhibition of global translation (**Figure 6G,H, supplementary figure 5C**). These observations therefore, establish the strong influence of AMPK over

497 receptor mediated translation regulation and highlights the importance of AMPK-eEF2

498 signaling axis in the same context.

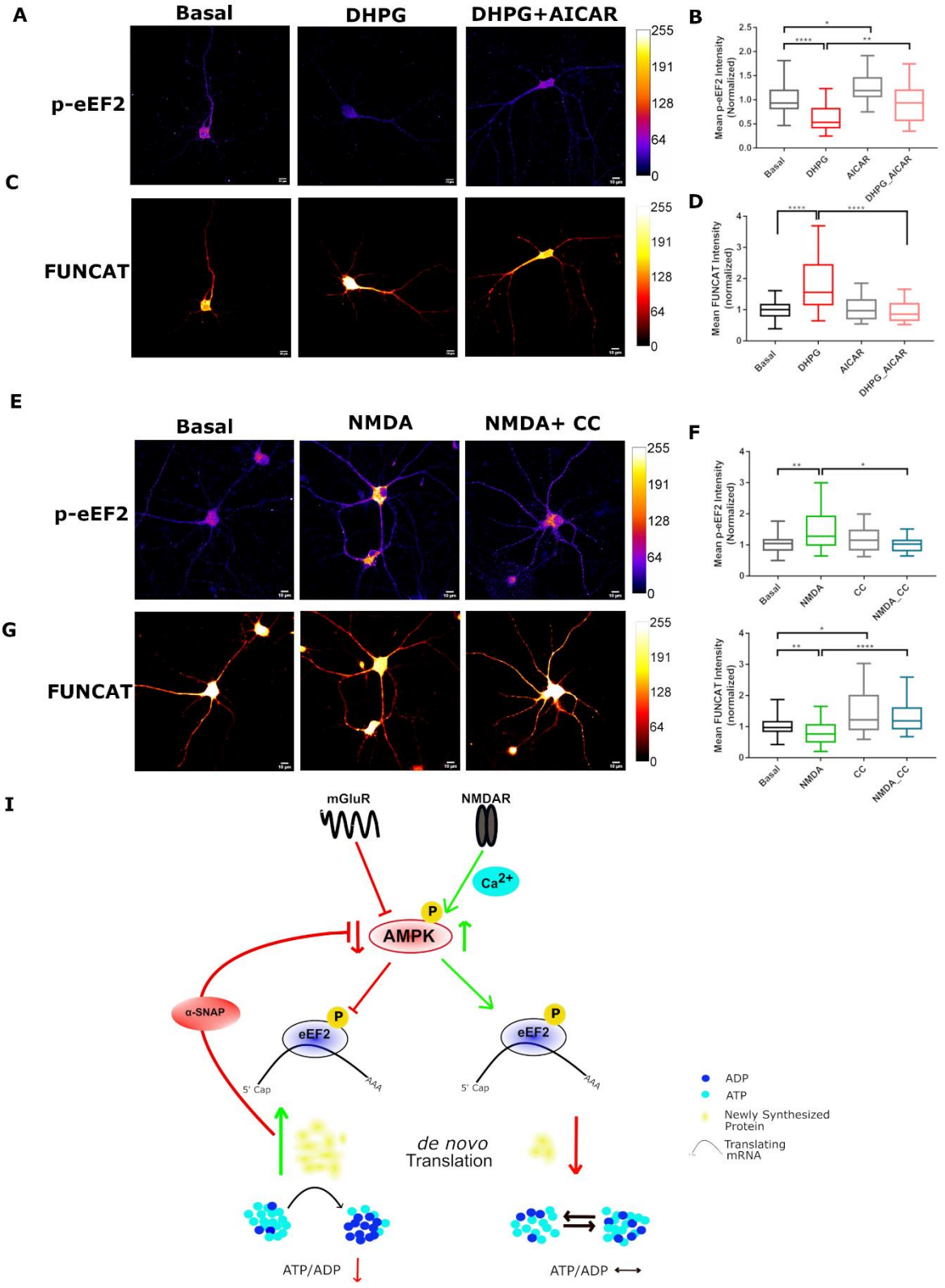

Figure 6:

Perturbation of AMPK Function Disrupts Receptor Specific Translation Response:

(A) Representative images showing phospho-eEF2 immunolabeling (Pseudo-colored) in cortical neurons on basal condition, on DHPG (50μM) treatment for 5 minutes in presence or absence of AICAR (1mM). MAP2B immunolabeling (supplementary figure 5B) was used for identifying neurons and intensity was used for normalization. Scale=10μM.

(B) Box plot showing phospho-eEF2 intensity distribution across multiple neurons on basal condition, on DHPG treatment for 5 minutes, on AICAR treatment for 1 hour and on DHPG treatment along with AICAR pre-treatment. *p<0.05, **p<0.01, ****p<0.0001, n=17-46 cells per group from 3 independent plating. One-way ANOVA followed by Bonferroni's multiple comparison test.

(C) Representative images showing newly synthesized proteins visualized through FUNCAT metabolic labeling (pseudo-colored) in cortical neurons under basal condition, on DHPG treatment for 5 minutes in presence or absence of AICAR. MAP2B immunolabeling (supplementary figure 5B) was used for identifying neurons and intensity was used for normalization. Scale=10μM.

(D) Box plot showing FUNCAT intensity distribution across multiple neurons on basal condition, on DHPG treatment for 5 minutes, on AICAR treatment for 1 hour and on DHPG treatment along with AICAR pre-treatment. ****p<0.0001, n=18-57 cells per group from 3 independent plating. Kruskal-Wallis test followed by Dunn's multiple comparison test.

(E) Representative images showing phospho-eEF2 immunolabeling (Pseudo-colored) in cortical neurons on basal condition, on NMDA (20μM) treatment for 5 minutes in presence or absence of

Compound C (10μM). MAP2B immunolabeling (supplementary figure 5B) was used for identifying neurons and intensity was used for normalization. Scale=10μM.

(F) Box plot showing phospho-eEF2 intensity distribution across multiple neurons on basal condition (Vehicle control), on NMDA treatment for 5 minutes, on Compound C pre-treatment for 1 hour and on NMDA treatment along with Compound C pre-treatment. *p<0.05, **p<0.01, n=21-36 cells per group from 3 independent plating. Kruskal-Wallis test followed by Dunn's multiple comparison test.

(G) Representative images showing newly synthesized proteins visualized through FUNCAT metabolic labeling (pseudo-colored) in cortical neurons under basal condition, on NMDA (20μM) treatment for 5 minutes in presence or absence of Compound C (1mM). MAP2B immunolabeling (supplementary figure 5C) was used for identifying neurons and intensity was used for normalization. Scale=10μM.

(H) Box plot showing FUNCAT intensity distribution across multiple neurons on basal condition, on NMDA treatment for 5 minutes, on Compound C treatment for 1 hour and on NMDA treatment along with Compound C pre-treatment. *p<0.05, **p<0.01, ****p<0.0001, n=24-52 cells per group from 3 independent plating. Kruskal-Wallis test followed by Dunn's multiple comparison test.

(G) Schematic showing receptor specific regulation of AMPK-eEF2 signaling and their subsequent impact on global translation. mGluR stimulation (Left) have been found to inactivate AMPK necessary for subsequent downregulation of eEF2 phosphorylation. This led to enhanced global *de-novo* translation and consumption of ATP, hence reducing neuronal ATP/ADP ratio. NMDAR stimulation (Right) caused activation of AMPK in extracellular Ca^{2+} dependent manner causing an increase in eEF2 phosphorylation in turn. This leads to inhibition of global translation therefore having no significant alterations in cellular ATP/ADP ratio.

Discussion:

In this work we present multiple lines of evidences showing activity induced protein synthesis contributes significantly to the energy expenditure in neurons on glutamate stimulation. Our work demonstrate that the global de-novo protein synthesis is dynamically regulated by mGluRs and NMDARs with distinct kinetics. As a consequence, we also observed dynamic alterations in energy level with characteristic temporal features specific to each type of stimulus. An AMPK-eEF2 signaling nexus combines uniquely to bring about the characteristic changes in translation with distinct mechanisms for each stimulus.

Protein Synthesis is the Major Energy Consumer on Glutamate Stimulation

It was predicted that activity dependent ATP consumption in neurons is largely due to the reversal of ionic fluxes (Harris, Jolivet, and Attwell 2012). Our study for the first time establishes the significant effect of activity induced protein synthesis on neuronal energy expenditure. Interestingly we failed to observe any noteworthy contribution from vesicle endocytosis at the pan-neuronal ATP level, unlike what has been observed previously in the axon terminals (Rangaraju, Calloway, and Ryan 2014). This demonstrates the distinct nature of energy regulations in various compartments as compared to that of the whole neurons.

mGluRs and NMDARs affect rate of global translation differently

We identified distinct roles for mGluRs and NMDARs in glutamate driven energy usage. Our results demonstrate mGluR dependent translation activation consumes significant amount of ATP and shares distinct kinetic features to that of NMDAR. Gp I mGluRs have

been widely reported to activate protein synthesis (Weiler et al. 2004)(Luchelli, Thomas, and Boccaccio 2015) and induce or facilitate long-term depression in excitatory synapses (Huber, Kayser, and Bear 2000) across various brain regions [reviewed in (Bellone, Lüscher, and Mameli 2008)(Schulte 2010)(Jörntell and Hansel 2006)]. Our results indicate that, mGluR mediated translation activation impact global, dendritic and synaptic energy level immediately. Contrarily, NMDAR stimulation accompanies a delayed impact on global, dendritic or synaptic ATP levels through a delayed translation activation as observed previously (Scheetz, Nairn, and Constantine-paton 2000).

The AMPK-eEF2 Signaling to Create Differential Response

Our results describe a key role for AMP activated protein Kinase in both mGluR and NMDAR mediated translation regulation. While AMPK is demonstrated to regulate activity induced energy metabolism (Marinangeli et al. 2018), sustained activity induced GLUT4 membrane expression in nerve terminals (Ashrafi et al. 2017) and various forms of synaptic plasticity (Potter et al. 2010)(Kong et al. 2016), our study provide mechanistic basis coupling its role on regulation of energy metabolism and translation. AMPK is known to influence eEF2 Kinase function either directly (Browne, Finn, and Proud 2004) or through indirect mechanisms involving inhibition of mTOR-S6K pathway (Inoki, Zhu, and Guan 2003), thereby regulating global translation. mGluR mediated inactivation of AMPK can thus also create opportunity for increased mTOR-S6K activity as observed previously (Hou 2004). These results therefore could explain the dephosphorylation of eEF2 downstream of mGluR stimulation, an effect unexplored previously. The fact that mGluR mediated AMPK activation is protein synthesis

591 dependent led to us investigate the role of AMPK specific phosphatase α-SNAP (Wang
592 and Brautigan 2013) in this context. Increased α-SNAP level and its association with
593 AMPK on mGluR stimulation suggestive of a feedback regulation of AMPK function.
594 NMDAR stimulation on the contrary involved Ca^{2+} dependent activation of AMPK
595 probably involving one of its upstream kinase CamKIIß. This collates well with the
596 enhanced phosphorylation of eEF2 on NMDA treatment (**supplementary figue 4D**) as
597 observed previously (Maus et al. 2006).

598 The study also clearly demonstrates the importance of protein synthesis in neuronal
599 energy budget particularly during neuronal activity. AMPK plays a pivotal role in
600 dictating this correlation. A deeper elucidation of this correlation would be of greater
601 significance in many pathophysiological conditions such as stroke, epilepsy and
602 neurodegenerative diseases. Unraveling other signaling mechanisms underlying the
603 connection between protein synthesis and energy dynamics and their long term effect
604 on synaptic plasticity may also provide potential therapeutic targets for diseases
605 involving impairment in energy metabolism and dysregulated protein synthesis.

606 ## Materials and Methods

607 **Ethics Statement:** All animal work was done in compliance with the procedures
608 approved by the Institutional Animal Ethics committee (IAEC) and the Institutional
609 Biosafety Committee (IBSC), InStem, Bangalore, India. All Work was done with Sprague
610 dawley (SD)rats. Rats were kept in 20-22'c temperature, 50-60 relative humidity, 0.3µm
611 HEPA filtered air supply at 15-20 ACPH and 14/10 light/dark cycle maintained. Food
612 and water were provided *ad libitum*.

Antibodies and Drugs: Anti-phospho eEF2 antibody (Thr 56; cat no: 2331; Used at 1:1000 dilution for western blotting analysis and 1:250 for immunocytochemistry), anti-eEF2 antibody (cat. no 2332; Used at 1:1000 dilution for western blotting analysis), Anti-phospho AMPKα antibody (Thr 172; cat. no: 2535; used at 1:500 dilution for western blotting analysis and 1:100 for immunocytochemistry analysis), anti-AMPK antibody (cat no: 2532; used at 1:1000 dilution for western blotting analysis), Anti-phospho ACC antibody (cat no: 3661; used at 1:1000 dilution for western blotting analysis) were obtained from Cell Signalling Technologies (MA, US). Anti- tubulin antibody (cat no: T9026; used at 1:1000 dilution for western blotting analysis), anti-MAP2B antibody (cat no: M9942; used at 1:500 dilution for immunocytochemistry), anti-rabbit HRP labelled secondary antibody (cat no: A0545 ; used at 1:5000 dilution for western blotting analysis), anti-mouse HRP labelled secondary antibody (cat no: A9044 ; used at 1:5000 dilution for western blotting analysis) were obtained from Sigma-Aldrich (St. Louis, MO). Anti-rabbit secondary antibody alexa 555 labelled (cat no: A11032; used at 1:500 dilution for immunocytochemistry) and anti-mouse secondary antibody alexa 488 labelled (cat no: A11008; used at 1:500 dilution for immunocytochemistry) were obtained from Thermo fisher Scientific (Waltham, MA). Anti-α-SNAP antibody (cat no: X1026; used at 1:1000 dilution for western blotting analysis). Glutamate (25μM), NMDA (20μM for neurons and 40μM for SNS), CNQX (40μM), Anisomycin (25μM for neurons and 50μM for synaptoneurosomes), Cycloheximide (100μg/ml), Ouabain octahydrate (1mM), Dynasore hydrate (100μM), Poly-L-Lysine (0.2mg/ml), Pluronic-F-127(0.002%), BAPTA (10mM) and Ionomycin (10μM) were obtained from Sigma-aldrich (St. Louis, MO). S-3,5 DHPG (20μM for neurons and 100μM for SNS), 5-aminoimidazole-4-carboxamide

ribonucleotide (AICAR, 1mM), D-AP5 (25μM), MK-801 (10μM) and mPEP (10μM) were obtained from Tocris Biosciences. Compound C (dorsomorphin; 40μM in synaptoneurosomes and 20μM in cultured neurons) were obtained from Santa Cruz Biotechnology (Santa Cruz, CA). Fuo-8 AM (2μM) was obtained from AAT Bioquest (Sunnyvale, CA).

Synaptoneurosome preparation Synaptoneurosomes were prepared from SD WT rat cortices at the age between post-natal day 28-33 (P28-33) following differential centrifugation method as described previously (Hollingsworth et al., 1985 Scheetz, Nairn, & Constantine-paton, 2000 R. S. Muddashetty, Kelic, Gross, Xu, & Bassell, 2007). Briefly, rat cortices were dissected and homogenized at 4°C in 8 volumes of synaptoneurosome (SNS) homogenization buffer [containing (in mM) 25 Tris-HCl pH 7.4, 118 NaCl, 4.7 KCl, 1.2 MgSO4, 2.5 CaCl2, 1.53 KH2PO4 and 212.7 glucose, , supplemented with Complete protease inhibitors (Roche)]. Homogenates were then passed through three 100μm nylon mesh filters followed by one 11μm filter MLCWP 047 Millipore (Bedford, MA) and centrifuged at 1000g for 20 minutes at 4°C. The pellet was resuspended into 2ml of the same buffer. In experiments with no Ca^{2+}, $CaCal_2$ was not added in the resuspension buffer. The resuspended SNS particles were then incubated at 37°C to make them metabolically active.

Synaptoneurosome Stimulation: For Stimulation, synaptoneurosomes were pre-warmed at 37°C for minimum of 5 minutes. A sample fraction aliquoted at this point was considered unstimulated condition or 0 min of stimulation for further analysis. This was followed by Gp I mGluR and NMDAR stimulation with specific agonists (s)3,5-dihydroxyphenylglycine (DHPG; 100μM) and N-methyl D-aspartate (NMDA; 40μM)

659 respectively. Further fractions were collected after 2 minutes and 5 minutes of
660 stimulation. A fraction was collected 5 minutes post-stimulation (5 min stimulation + 5
661 min recovery). For this, the synaptoneurosomes were first stimulated for 5 minutes with
662 agonists. This is followed by removal of the stimulus through centrifugation at 13,000g
663 for 20 seconds and resuspension with 37°C pre-warmed synaptoneurosome
664 homogenization buffer. These synaptoneurosomes were further incubated for 5 minutes
665 and processed for ATP measurement, protein estimation and western blot analysis. For
666 ATP measurements, stimulation was terminated by direct lysis of synaptoneurosomes
667 with equal volume of boiling water (Yang et al. 2002). This was followed by
668 centrifugation at 20,000g for 2.5 minutes for the measurement of soluble ATP content
669 from the supernatant. For protein estimation and western blot analysis,
670 synaptoneurosomes fractions were centrifuged at 13,000g for 20 seconds followed by
671 lysing with lysis buffer [containing:] (**Stimulation protocol figure 2F**). In experiments
672 involving pre-treatment of drugs, pre-warming period varied depending on the
673 incubation period of various drugs which were directly added after the resuspension
674 step. Untreated control synaptoneurosomes were pre-incubated for same period as drug
675 pre-treatment time for comparisons.

676 **Cell line and primary neuronal culture** Primary neurons were cultured from cerebral
677 cortices as described by Banker & Goslin, 1998. Embryos were obtained from females
678 at the 18th day of gestation period (E18) and cerebral cortices were dissected out in ice
679 cold Hank's balanced salt solution under a dissection microscope. Cells were dissociated
680 with 0.25% trypsin solution at 37°C for 10 minutes followed by mechanical trituration
681 in minimal essential medium (MEM, Thermo fisher) with 10% foetal bovine serum

682 (sigma). Dissociated cells were plated on tissue culture dishes or coverslips coated with
683 poly-L-lysine (0.2 mg/ml in borate buffer, pH 8.5). Neurons were attached to the
684 substrate in MEM with 10% FBS for 3h, followed by defined Neurobasal Medium
685 (Invitrogen) with GlutaMAX™ supplement (Gibco™) and B-27 supplements (Invitrogen)
686 for 14 days at 37˚C in a 5% CO_2 environment. For immunocytochemistry, cells plated on
687 coverslips kept in a 10cm diameter tissue culture dish with a plating density of 10^5
688 cells/dish. The coverslips are then inverted onto astroglial bed in neurobasal media
689 after substrate attachment in MEM. For biochemical and immunoblotting experiments,
690 cells were grown on 6 well dishes or 35mm diameter dishes with seeding density
691 $4X10^5$/well. For live imaging experiments, cells were seeded with $2X10^5$/35mm
692 diameter glass bottom dishes.

693 **Metabolic Labelling:** For metabolic labelling of proteins, neurons were incubated for 1
694 hour in methionine-free Dulbecco's Modified Essential Medium (DMEM, Thermo Fisher).
695 This was followed by addition of L-azidohomoalanine (AHA; 1μM) for next 55 minutes in
696 the same medium. At this point a group of cells were fixed with 4% Paraformaldehyde
697 (PFA) for 20 minutes and would be considered as unstimulated basal for further analysis.
698 This was followed by either fixing the cells with 4% PFA or the cells were stimulated
699 with mGluR and NMDAR specific agonists DHPG (50uM) and NMDA (20 uM) respectively
700 for 2 minutes, 5 minutes or post stimulation 5 minutes recovery (5 min stim + 5 min
701 recovery) and subsequently fixed with 4% PFA. Cells were then permeabilized in TBS_{50}
702 [containing (in mM):50 Tris-Base, 150 NaCl] + 0.3% Triton X 100 solution and blocked
703 using TBS_{50} + 0.1% Triton X 100 + 2% BSA + 4% FBS containing blocking solution. Newly
704 synthesized proteins were then labeled with Alexa-Fluor-555–alkyne [Alexa Fluor 488 5-

carboxamido-(propargyl), bis (triethylammonium salt)], by allowing the fluorophore alkyne to react with AHA azide group through click chemistry. All reagents were from Thermo Fisher and stoichiometry of reagents were calculated according to the suggested manual by the manufacturer (CLICK-iT cell reaction buffer kit, cat.no. C10269). Signal intensity was then measured using confocal microscopy to calculate the amount of newly synthesized proteins. For specific detection of neuronal cells, MAP2B positive cells were used for analysis.

Immunocytochemistry: Rat primary cortical neurons were stimulated with either 50µM DHPG or 20µM NMDA for 5mins. Cells were fixed with 4% PFA and processed for imaging as described before. In brief, cells were permeabilized using TBS_{50} + 0.3% T solution and were treated with Tris-Glycine solution (containing in Moles: 0.5 Tris-base and 0.2 Glycine) before blocking with blocking buffer [TBS_{50} + 0.1% T) + 2% BSA + 4% FBS]. Primary antibodies were incubated in blocking buffer overnight at 4°C under gentle shaking condition followed by washes. Alexa Fluor 488 coupled anti-mouse and Alexa Fluor 555 coupled anti-rabbit secondary antibodies were incubated for 2h at room temperature. Finally, coverslips were mounted for imaging using Mowiol® 4-88 mounting media. Images were acquired on a Leica TCS SP5 confocal microscope (Leica Biosystems) with HCX PL APO 63X, NA 1.4, oil immersion objective. Imaging conditions were kept constant across groups. Images were acquired on Olympus FLUOVIEW 3000 confocal laser scanning microscope (Olympus Corporation) with HCX PL APO 60x, NA 1.4, oil immersion objective. For quantification of fluorescence intensities, images were acquired while keeping the open pinhole configuration to collect lights from planes below and above the focal plane as well. Objective was moved in the Z direction

with a step size of 0.5µm for 12 such steps to ensure the light was collected from the entire cell across its thickness. For quantification of colocalization, images were acquired using 2.5x optical zooming of to satisfy Nyquist's sampling theorem of information theory for maximum resolution in the XY direction. Pinhole was kept at 1 Airy unit to ensure optimum resolution and confocal stacks were acquired with a step size of 0.3µm calculated based on the fluorophore wavelength. Imaging conditions were kept constant across different data sets, across experiments.

Live Cell fluorescence Microscopy:

Imaging Dendritic ATP/ADP Ratio: Cells were imaged on Zeiss LSM 780 confocal laser scanning microscope (Car Zeiss, Oberkochen, Germany) with 63X Zeiss plan-apochromat oil immersion objective, NA 1.4 with argon lasers of specified wavelength. Cells were grown in Neurobasal media containing B27 supplements and Glutamax and were transfected with PercevalHR and pH-Red construct for simultaneous monitoring of intracellular ATP/ADP ratio and pH. pH monitoring was done as suggested in previous studies (Tantama and Yellen 2014) to correct for the bias created in Perceval HR fluorescence solely due to the change in intracellular pH. Perceval HR was excited with 488/20 nm and 405/20 nm band-pass filters and emission was collected through a 520/15nm band-pass filter. Excitation and emission beams were separated through 490 nm short pass dichroic mirror. pH-Red was excited using 561/20nm and 455/10 nm band-pass filters and emission was collected through 630/50 nm band pass filter. A 560 nm short-pass dichroic was used to separate excitation and emission beams.

Neurons were imaged at room temperature in 37°C pre-warmed Neurobasal media without phenol red (Thermo Fisher, Waltham, MA, USA) containing 15mM HEPES. For,

approximate pH bias removal, the linear relationship established between Perceval HR and pH-Red fluorescence for the high glucose 'ATP Loaded' state by Tantama et. Al., 2014 was used. The relationship was used to predict the pH bias of Perceval HR signal from the continuously monitored pH-Red signal and was normalized to the observed Perceval HR fluorescence for the entire period of experiment. Images were captured at 16-bit image format with 512X512 pixel distribution with frame rate of 1 per 15 seconds.

Ca^{2+} Imaging: Growth media from cells grown on glass bottom petri dishes were first removed and were washed with imaging media [containing in mM: 120 NaCl, 3 KCl, 2 CaCl2, 1MgCl2, 3 NaHCO3, 1.25 NaH2PO4, 15 HEPES, 30 glucose (pH 7.4). They were then incubated with 2 ml freshly prepared dye solution (2 μM Fluo-8 AM and 0.002% Pluronic F-127 in imaging media) at 37°C for 10 mins followed by a 5 minutes incubation procedure at the same temperature with the imaging media. They were then imaged on Olympus FV3000 confocal laser scanning inverted microscope with 20X air objective lens NA 0.75, illuminated with 488nm solid state lasers. Images were acquired at a rate of single frame per 3.22 sec intervals at room temperature. Cells were imaged for 322 sec (100 frames) for recording spontaneous activity, followed by 644 sec (200 frames) with stimulant and 161 sec (50 frames) with KCl (to check neuronal activity) or ionomycin (F_{max}). After background, fluorescence were calibrated to $[Ca^{2+}]_i$ as $[Ca^{2+}]_i$ = 389 $(F-F_{min})/(F_{max}-F)$nM. F_{min} was recorded by chelating Ca^{2+} with 10μM ionomycin (Calbiochem) and 10mM BAPTA (Sigma) in independent experiments and F_{max} was recorded by 10μM ionomycin in presence of 2.5mM $CaCl_2$ in each experiment.

773 **Luciferase Assay:** To measure synaptic ATP levels, Cortical synaptoneurosomes were
774 first pre-warmed and then stimulated with Gp I mGluR and NMDAR specific agonists at
775 37°C under constant shaking. Fractions of the stimulated solutions were collected at
776 time points specified before. For treatment with various drugs, the pre-warming period
777 varied depending on the pre-incubation time of the drug before the stimulants were
778 added. Collected fractions were added to equal volume of boiling water to extract the
779 ATP as described previously (Yang et al., 2002). The lysates were then used for
780 quantification of soluble ATP molecules using luciferase based commercial ATP
781 quantification kit (ATP Determination kit, Thermo fisher, Cat.no. A22066) with the help
782 of a standard curve. For measuring ATP/ADP ratio from cortical neurons, cells were
783 stimulated for specified time points and lysed with lysis buffer [containing in mM: 50
784 Tris-Cl (pH-7.4), 150 NaCl, 5 $MgCl_2$, 1% Triton-X-100, supplemented with EDTA free
785 protease inhibitor complex (Sigma, cat. no. S8830) and phosphatase inhibitor cocktail
786 (Roche, ref.no. 04906837001)]. Lysates were then centrifuged at 20,000g for 20 minutes
787 and supernatants were used for measuring ATP using luciferase-based protocol. This
788 was followed by a step converting ADP to ATP which was then used to measure the ATP
789 and ADP level together constituting majority of the adenine nucleotides. This was done
790 using a commercially available luminescence-based kit (ADP/ATP ratio kit, Abcam,
791 cat.no. ab65313) following the user manual suggested by the manufacturer.

792 **Image Analysis:** Image analysis was done using Fiji (ImageJ based image processing
793 package) and IMARIS 9.0 (Bitplane, Oxford instrument company, Belfast, UK) software.
794 For fluorescence intensity quantification, confocal stacks were collapsed using sum
795 slice projection method and mean intensity was quantified from the cells. MAP2B

positive cells were used for identification of neurons and quantified mean intensity values were used for normalization. For quantifying co-localization, Pearson's correlation coefficient (PCC) was measured for the cell body and proximal dendrite region (<50µm). For the coefficient analysis, measurement was done after manual thresholding with threshold value of 155 for a 12bit image format. For time frame analysis, mean fluorescence intensity was quantified for the imaged dendritic region from each time frame. Time frame analysis was done using the time series analyser V3 plug in from Fiji. Representative images for ratiometric quantifications were generated using the Ratio Plus plug from Fiji where the image was generated by calculating pixel by pixel intensity ratio between two channels.

Statistical Analysis: Statistical comparisons were done using GraphPad Prism (Prism 7.01, Graphpad Software Inc, La Jolla, CA, USA). For group comparisons, the data distributions were first tested for normality using Kolmogorov-Smirnov Goodness-of-Fit Test or Shapiro-Wilk normality test. Depending on the distribution, either parametric or non-parametric tests were used to quantify statistical significance. For groups with <4 data points, the inherent distribution was considered to follow Gaussian distribution unless mentioned. For comparing two groups, Student's t test (two tailed, paired/unpaired) was done to calculate statistical significance. Multiple group comparisons were made using one-way ANOVA followed by Bonferroni's multiple comparison test for parametric distribution and Kruskal-Wallis's Test followed by Dunn's Multiple comparison test. Two-way ANOVA followed by Holm Sidak's multiple comparison test was performed for comparing multiple groups at various time points.

818 Data are presented as mean ± SEM. p values < 0.05 was considered statistically
819 significant.

820 **Acknowledgement**

821 We are thankful to Central Imaging and Flow-cytometry Facility (CIFF) for LSM 780 and
822 FV3000 confocal microscopes, NCBS animal house facility for generously maintingng the
823 rat colony needed for experimentation. We extend our gratitude to Professor M.K.
824 Mathew and Dr. Tina Mukherjee for their helpful comments and discussion. We thanks
825 Chaitra Ananda, Amirthavarshini Devrajan and Sonu. P. Kurien for their gracious efforts
826 in experimental support and data analysis. The work was supported by the Neurostem
827 grant (BT/IN/Denmark/07/RSM/2015-2016) and Center for Brain Development and
828 Repair (CBDR) (BT/MB-CNDS/2013), Department of Biotechnology, Govt. of India. We
829 thank Dr. Garry Yellen, Harvard University for his useful suggestions on PercevalHR
830 experiments.

831 **Author contribution**

832 S.G.D designed and performed the experiments, analyzed data and co-wrote the
833 manuscript. Sumita.C performed Calcium imaging experiments and analyzed data,
834 Sumantra C. provided resources, A.B provided resources and analyzed data, R.M
835 designed experiments and co-wrote manuscripts.

836 **References**

837 Ashrafi, Ghazaleh, Zhuhao Wu, Ryan J. Farrell, and Timothy A. Ryan. 2017. “GLUT4
838 Mobilization Supports Energetic Demands of Active Synapses.” *Neuron* 93(3): 606–
839 615.e3.

840 Attwell, David, and Simon B. Laughlin. 2001. “An Energy Budget for Signaling in the
841 Grey Matter of the Brain.” *Journal of Cerebral Blood Flow and Metabolism*
842 21(10): 1133–45.

843 Banker, Gary, and Kimberly Goslin. 1998. “Culturing Nerve Cells.” In *Cellular and*
844 *Molecular Neuroscience Series*, , 666.

845 Bellone, C., C. Lüscher, and M. Mameli. 2008. “Mechanisms of Synaptic Depression
846 Triggered by Metabotropic Glutamate Receptors.” *Cellular and Molecular Life*
847 *Sciences* 65(18): 2913–23.

848 Browne, Gareth J., Stephen G. Finn, and Christopher G. Proud. 2004. “Stimulation of
849 the AMP-Activated Protein Kinase Leads to Activation of Eukaryotic Elongation
850 Factor 2 Kinase and to Its Phosphorylation at a Novel Site, Serine 398.” *Journal of*
851 *Biological Chemistry* 279(13): 12220–31.

852 Burkewitz, Kristopher, Yue Zhang, and William B. Mair. 2014. “AMPK at the Nexus of
853 Energetics and Aging.” *Cell Metabolism* 20(1): 10–25.
854 http://dx.doi.org/10.1016/j.cmet.2014.03.002.

855 Dieterich, Daniela C. et al. 2010. “In Situ Visualization and Dynamics of Newly
856 Synthesized Proteins in Rat Hippocampal Neurons.” *Nature Neuroscience* 13(7):
857 897–905. http://dx.doi.org/10.1038/nn.2580.

858 Harris, Julia J., Renaud Jolivet, and David Attwell. 2012. “Synaptic Energy Use and
859 Supply.” *Neuron* 75(5): 762–77. http://dx.doi.org/10.1016/j.neuron.2012.08.019.

860 Hawley, Simon A. et al. 1996. “Characterization of the AMP-Activated Protein Kinase

Kinase from Rat Liver and Identification of Threonine 172 as the Major Site at Which It Phosphorylates AMP-Activated Protein Kinase." *Journal of Biological Chemistry* 271(44): 27879–87.

Hollingsworth, E B et al. 1985. "Biochemical Characterization of a Filtered Synaptoneurosome Preparation from Guinea Pig Cerebral Cortex: Cyclic Adenosine 3':5'-Monophosphate-Generating Systems, Receptors, and Enzymes." *The Journal of neuroscience* 5(8): 2240–53. http://www.ncbi.nlm.nih.gov/pubmed/2991484.

Hou, L. 2004. "Activation of the Phosphoinositide 3-Kinase-Akt-Mammalian Target of Rapamycin Signaling Pathway Is Required for Metabotropic Glutamate Receptor-Dependent Long-Term Depression." *Journal of Neuroscience* 24(28): 6352–61. http://www.jneurosci.org/cgi/doi/10.1523/JNEUROSCI.0995-04.2004.

Huber, Kimberly M, Matthew S Kayser, and Mark F Bear. 2000. "Role for Rapid Dendritic Protein Synthesis in Hippocampal Depression." *Science* 288(May): 1254–56.

Hunt, David L., and Pablo E. Castillo. 2012. "Synaptic Plasticity of NMDA Receptors: Mechanisms and Functional Implications." *Current Opinion in Neurobiology* 22(3): 496–508.

Inoki, Ken, Tianqing Zhu, and Kun-Liang Guan. 2003. "TSC2 Mediates Cellular Energy Response to Control Cell Growth and Survival Phosphorylation Decreases the Ability of TSC2 to Inhibit the Phosphorylation of Ribosomal S6 Kinase (S6K) and Eukaryotic Initiation Factor 4E Binding Protein-1 (4EBP1)." *Cell* 115(5): 577–90.

883 Jörntell, Henrik, and Christian Hansel. 2006. "Synaptic Memories Upside Down:
884 Bidirectional Plasticity at Cerebellar Parallel Fiber-Purkinje Cell Synapses."
885 *Neuron* 52(2): 227–38.

886 Koenig, Jenny B, and Chris G Dulla. 2018. "Dysregulated Glucose Metabolism as a
887 Therapeutic Target to Reduce Post-Traumatic Epilepsy." *Frontiers in cellular*
888 *neuroscience* 12(October): 350.
889 http://www.ncbi.nlm.nih.gov/pubmed/30459556%0Ahttp://www.pubmedcentral
890 .nih.gov/articlerender.fcgi?artid=PMC6232824.

891 Kong, Dong et al. 2016. "A Postsynaptic AMPK→p21-Activated Kinase Pathway Drives
892 Fasting-Induced Synaptic Plasticity in AgRP Neurons." *Neuron* 91(1): 25–33.

893 Luchelli, L., M. G. Thomas, and G. L. Boccaccio. 2015. "Synaptic Control of MRNA
894 Translation by Reversible Assembly of XRN1 Bodies." *Journal of Cell Science*
895 128(8): 1542–54. http://jcs.biologists.org/cgi/doi/10.1242/jcs.163295.

896 Malenka, Lüscher; 2012. "NMDA Receptor-Dependent Long-Term Potentiation and
897 Long-Term Depression (LTP/LTD)." : 1–16.
898 https://www.semanticscholar.org/paper/Depression-(-LTP-%2F-LTD-)-NMDA-
899 Receptor-Dependent-Sabatini-
900 Weinberg/17a6e1f48986de2c5553846603b49acf1ce70578.

901 Manlio Díaz-García, Carlos et al. 2017. "Neuronal Stimulation Triggers Neuronal
902 Glycolysis and Not Lactate Uptake Cell Metabolism Article Neuronal Stimulation
903 Triggers Neuronal Glycolysis and Not Lactate Uptake." *Cell Metabolism* 26: 361–
904 374.e4. http://dx.doi.org/10.1016/j.cmet.2017.06.021.

905 Marinangeli, Claudia et al. 2018. "AMP-Activated Protein Kinase Is Essential for the
906 Maintenance of Energy Levels during Synaptic Activation." *iScience* 9: 1–13.
907 https://linkinghub.elsevier.com/retrieve/pii/S2589004218301652.

908 Maus, M. et al. 2006. "2-Deoxyglucose and NMDA Inhibit Protein Synthesis in Neurons
909 and Regulate Phosphorylation of Elongation Factor-2 by Distinct Mechanisms."
910 *Journal of Neurochemistry* 96(3): 815–24.

911 Mink, J. W., R. J. Blumenschine, and D. B. Adams. 1981. "Ratio of Central Nervous
912 System to Body Metabolism in Vertebrates: Its Constancy and Functional Basis."
913 *American Journal of Physiology-Regulatory, Integrative and Comparative*
914 *Physiology* 241(3): R203–12.
915 http://www.physiology.org/doi/10.1152/ajpregu.1981.241.3.R203.

916 Muddashetty, R. S. et al. 2007. "Dysregulated Metabotropic Glutamate Receptor-
917 Dependent Translation of AMPA Receptor and Postsynaptic Density-95 MRNAs at
918 Synapses in a Mouse Model of Fragile X Syndrome." *Journal of Neuroscience*
919 27(20): 5338–48. http://www.jneurosci.org/cgi/doi/10.1523/JNEUROSCI.0937-
920 07.2007.

921 Pathak, Divya et al. 2015. "The Role of Mitochondrially Derived ATP in Synaptic
922 Vesicle Recycling." *Journal of Biological Chemistry* 290(37): 22325–36.

923 Pedersen, Stine F. et al. 1998. "Mechanisms of PH(i) Regulation Studied in Individual
924 Neurons Cultured from Mouse Cerebral Cortex." *Journal of Neuroscience*
925 *Research* 51(4): 431–41.

926 Potter, Wyatt B. et al. 2010. "Metabolic Regulation of Neuronal Plasticity by the

927 Energy Sensor AMPK." *PLoS ONE* 5(2).

928 Rangaraju, Vidhya, Nathaniel Calloway, and Timothy A. Ryan. 2014. "Activity-Driven
929 Local ATP Synthesis Is Required for Synaptic Function." *Cell* 156(4): 825–35.
930 http://dx.doi.org/10.1016/j.cell.2013.12.042.

931 Rangaraju, Vidhya, Marcel Lauterbach, and Erin M. Schuman. 2019. "Spatially Stable
932 Mitochondrial Compartments Fuel Local Translation during Plasticity." *Cell* 176(1–
933 2): 73–84.e15. https://linkinghub.elsevier.com/retrieve/pii/S0092867418316271.

934 Rangaraju, Vidhya, Susanne tom Dieck, and Erin M Schuman. 2017. "Local Translation
935 in Neuronal Compartments: How Local Is Local?" *EMBO reports* 18(5): 693–711.
936 http://embor.embopress.org/lookup/doi/10.15252/embr.201744045.

937 Richter, Joel D., and Jeff Coller. 2015. "Pausing on Polyribosomes: Make Way for
938 Elongation in Translational Control." *Cell* 163(2): 292–300.
939 http://dx.doi.org/10.1016/j.cell.2015.09.041.

940 Rooijackers, Hanne M.M. et al. 2016. "Brain Glucose Metabolism during Hypoglycemia
941 in Type 1 Diabetes: Insights from Functional and Metabolic Neuroimaging
942 Studies." *Cellular and Molecular Life Sciences* 73(4): 705–22.

943 Ryazanov, Alexey G., and Elena K. Davydova. 1989. "Mechanism of Elongation Factor
944 2 (EF-2) Inactivation upon Phosphorylation Phosphorylated EF-2 Is Unable to
945 Catalyze Translocation." *FEBS Letters* 251(1–2): 187–90.

946 Scheetz, A J, Angus C Nairn, and Martha Constantine-paton. 2000. "NMDA Receptor-
947 Mediated Control Of." : 211–16.

948 Schulte, Gunnar. 2010. “The Class Frizzled Receptors.” *Pharmacological reviews*
949 62(4): 632–67. http://pharmrev.aspetjournals.org/content/61/4/395.short.

950 Schurr, Avital. 2002. “Lactate, Glucose and Energy Metabolism in the Ischemic Brain
951 (Review).” *International journal of molecular medicine* 10(2): 131–36.

952 Schwanhüusser, Björn et al. 2011. “Global Quantification of Mammalian Gene
953 Expression Control.” *Nature* 473(7347): 337–42.

954 Sutton, Michael A. et al. 2007. “Postsynaptic Decoding of Neural Activity: EEF2 as a
955 Biochemical Sensor Coupling Miniature Synaptic Transmission to Local Protein
956 Synthesis.” *Neuron* 55(4): 648–61.

957 Takei, Nobuyuki et al. 2009. “Brain-Derived Neurotrophic Factor Enhances the Basal
958 Rate of Protein Synthesis by Increasing Active Eukaryotic Elongation Factor 2
959 Levels and Promoting Translation Elongation in Cortical Neurons.” *Journal of*
960 *Biological Chemistry* 284(39): 26340–48.

961 Tantama, Mathew, Juan Ramón Martínez-François, Rebecca Mongeon, and Gary
962 Yellen. 2013. “Imaging Energy Status in Live Cells with a Fluorescent Biosensor of
963 the Intracellular ATP-to-ADP Ratio.” *Nature Communications* 4(May).

964 Tantama, Mathew, and Gary Yellen. 2014. 547 Methods in Enzymology *Imaging*
965 *Changes in the Cytosolic ATP-to-ADP Ratio*. 1st ed. Elsevier Inc.
966 http://dx.doi.org/10.1016/B978-0-12-801415-8.00017-5.

967 Vallée, Alexandre, Yves Lecarpentier, Rémy Guillevin, and Jean Noël Vallée. 2018.
968 “Demyelination in Multiple Sclerosis: Reprogramming Energy Metabolism and

Potential PPARγ Agonist Treatment Approaches." *International Journal of Molecular Sciences* 19(4).

Wang, Lifu, and David L. Brautigan. 2013. "α-SNAP Inhibits AMPK Signaling to Reduce Mitochondrial Biogenesis and Dephosphorylates Thr172 in AMPKα in Vitro." *Nature Communications* 4: 1559. http://dx.doi.org/10.1038/ncomms2565.

Weiler, Ivan Jeanne et al. 2004. "Fragile X Mental Retardation Protein Is Necessary for Neurotransmitter-Activated Protein Translation at Synapses." *Proceedings of the National Academy of Sciences of the USA* 101(50): 17504–9. http://www.pubmedcentral.nih.gov/articlerender.fcgi?artid=536018&tool=pmcentrez&rendertype=abstract.

Yang, Nae Cherng, Wai Meng Ho, Yu Hsuan Chen, and Miao Lin Hu. 2002. "A Convenient One-Step Extraction of Cellular ATP Using Boiling Water for the Luciferin-Luciferase Assay of ATP." *Analytical Biochemistry* 306(2): 323–27.

Supplementary Information

Supplementary Figure 1:

Quantifying Activity dependent changes in energy level. (Related to Figure 1)

(A) Bar graph representing normalized average value of neuronal ATP/ATP+ADP ratio in basal condition and on DHPG (50μM) and NMDA (20μM) treatment for 5 minutes. *p<0.05, n=3 independent plating. One-way ANOVA followed by Bonferroni's multiple comparison test.

(B) Bar graph representing normalized average value of neuronal ATP/ATP+ADP ratio in basal condition, on dynasore (100μM) treatment for 30 minutes, on Glutamate (25μM) treatment for 5 minutes and on glutamate treatment along with dynaosre pre-treatment. *p<0.05, n=3-6 independent plating. One-way ANOVA followed by Bonferroni's multiple comparison test.

(C) Quantification showing the effect of treatment of anisomycin, cycloheximide and MPEP on synaptic ATP level measured from cortical synaptoneurosomes. Data = mean ± SEM with scattered data points.

Supplementary Figure 2:

Sensor Calibration and Basal ATP measurement. (Related to Figure 2)

(A) Graph depicting a linear relationship was established between the percevalHR fluorescence ratio and the pH-Red fluorescence ratio using NH_4Cl pre-pulse method following method established previously (Pederson et. al, 1998, Tantama et. al, 2013). Briefly a gradient of 5-15mM NH_4Cl solution was applied to allow the changes in intracellular pH in a short period of time to avoid any metabolic stress. Changes in PercevalHR fluorescence was measured along with pH-Red fluorescence and the linear relation was used to remove pH bias approximately.

(B) Representative dendrite showing the temporal profile of PercevalHR fluorescence (ATP/ADP) in unstimulated condition. Scale=10μM.

(C) Average time traces showing the change in the dendritic ATP/ADP ratio on unstimulated condition in presence or absence of anisomycin. Data= mean ± SEM. n≥3 cells from independent platings per group.

(D) Quantification showing the changes in synaptic ATP level on unstimulated conditions. Data= mean ± SEM. n= 4 animals.

Supplementary Figure 3:

Translation Kinetics. (Related to Figure 3)

(A) Representative images showing newly synthesized proteins visualized through FUNCAT metabolic labeling (pseudo-colored) in cortical neurons at various time points in unstimulated condition. Absence of AHA while metabolic labeling was used as a negative control. MAP2B immunolabeling (green, inset) was used for identifying neurons and intensity was used for normalization. The average trace quantification and data point distribution for unstimulated cells have been presented in Figure 3C and 3D. Scale=10μM.

(B) Representative images showing immunolabeling of MAP2B (green) in cortical neurons at various time points following DHPG and NMDA treatment for the cells used for FUNCAT intensity quantification. Scale=10μM.

(C) Representative images showing immunolabeling of MAP2B (green) in cortical neurons in basal condition and DHPG and NMDA treatment for 5 minutes for the cells used for p-eEF2 quantification. Scale=10μM.

(D) Representative immunoblots describing changes in phospho-eEF2 and total-eEF2 levels at various time points after DHPG (50μM) and NMDA (20μM) treatment to cultured cortical neurons. Note in each case phospho and total eEF2 levels were normalized individually to tubulin before calculating the ratio.

(E) Line graph showing average value for neuronal phospho/total ratio of eEF2 at various time points after DHPG and NMDA treatment and 5 minutes and 10 minutes after recovery. Data:

mean +/- SEM, *p<0.05, **p<0.01, ***p<0.001, n= 3 animals per group. Two Way ANOVA followed by Bonferroni's multiple comparison test.

Supplementary Figure 4:

Baseline eEF2 phosphorylation and Characterization of NMDAR dependent Ca^{2+} entry. (Related to Figure 4 and Figure 5)

(A) Representative images showing immunolabeling of MAP2B (green) in cortical neurons in basal condition and DHPG and NMDA treatment for 5 minutes for the cells used for p-AMPK quantification. Scale=10μM.

(B) Line graph showing average value for synaptic phospho/total ratio of eEF2 and AMPK at various time points after DHPG and NMDA treatment and 5 minutes after recovery in cortical synaptoneurosomes. Data: mean +/- SEM, n≥ 2 animals per group. Two Way ANOVA followed by Bonferroni's multiple comparison test.

(C) Representative images depicting intracellular Ca^{2+} levels (Pseudo-colored) of a cortical neuron before stimulation, immediately (15s) after NMDA (20μM) treatment, at a later time point (300sec) after NMDA treatment and after ionomycin treatment along with 10mM Ca^{2+} in presence MK-801. Scale=20μM.

(D) Representative immunoblots describing changes in phospho-eEF2 and total-eEF2 levels at various time points after NMDA (40μM) treatment to cortical synaptoneurosomes in presence or absence of extracellular Ca^{2+}. Note in each case phospho and total AMPK levels were normalized individually to tubulin before calculating the ratio.

(E) Line graph showing average value for synaptic phospho/total ratio of eEF2 at various time points after NMDA treatment and 5 minutes after recovery in presence or absence of Ca^{2+}. Data:

mean +/- SEM, *p<0.05, **p<0.01, n≥ 4 animals per group. Two Way ANOVA followed by Bonferroni's multiple comparison test.

Supplementary Figure 5:

AMPK perturbations: (related to figure 6)

(A) Representative images showing phospho-eEF2 immunolabeling (Pseudo-colored), newly synthesized protein through FUNCAT metabolic labeling and MAP2B immunolabeling in cortical neurons on AICAR (1mM) treatment and Compound C (10μM) treatment for 1 hour. MAP2B immunolabeling was used for identifying neurons and intensity was used for normalization. Scale=10μM.

(B) Representative images showing immunolabeling of MAP2B (green) in cortical neurons in basal condition and on DHPG treatment for 5 minutes in presence or absence of AICAR for the cells used for p-eEF2 and FUNCAT quantification. Scale=10μM.

(C) Representative images showing immunolabeling of MAP2B (green) in cortical neurons in basal condition and on NMDA treatment for 5 minutes in presence or absence of Compound C for the cells used for p-eEF2 and FUNCAT quantification. Scale=10μM.